Intrinsic and extrinsic effects on the fracture toughness of ductile metallic glasses

Hong Li [a], Qing-Xiang Pei [b], Zhen-Dong Sha [a,*], Paulo S. Branicio [c,]**

[a] State Key Laboratory for Strength and Vibration of Mechanical Structures, School of Aerospace Engineering, Xi'an Jiaotong University, Xi'an 710049, China

[b] Institute of High Performance Computing, A*STAR, Singapore 138632, Singapore

[c] Mork Family Department of Chemical Engineering and Materials Science, University of Southern California, 3651 Watt Way, Los Angeles, CA 90089, United States

Abstract

The potential application of metallic glasses (MGs) as structural materials demands accurate measurements of their toughness and the understanding of the underlying factors affecting it. Currently, it is challenging to precisely measure the toughness of MGs, especially ductile MGs. Measured toughness values are widely scattered, even for MGs with identical compositions. That is attributed to the combined effect of intrinsic and extrinsic factors including processing, sample geometries, and loading conditions. A fundamental understanding of the influences of these elements is thus of great significance. In the present study, molecular dynamics simulations are performed to investigate the influence of intrinsic and extrinsic effects on the fracture toughness of CuZr MGs. In particular, focused is placed on the effects of cooling rate, notch shape and size, strain rate, and temperature. The results indicate that the fracture

* Corresponding authors.
E-mail address: zhendongsha@mail.xjtu.edu.cn (Z.-D. Sha), branicio@usc.edu (P.S. Branicio)

toughness of a MG scales with the cooling rate used to prepare it. This is attributed to increased free volume content generated at high cooling rates, which enhances plastic deformation and amplifies the associated energy dissipation during plastic deformation events. Fracture toughness also increases with the strain rate, arguably due to strain rate-induced crack extension delay. Overall, the results demonstrate that the largest fracture toughness are achieved when MG samples are fabricated at high cooling rates and subjected to high strain rate deformation. In addition, results suggest that the fracture toughness decreases with increasing temperature, due to the significant decrease in strength. The correlations revealed between these crucial intrinsic and extrinsic parameters and the calculated MG fracture toughness support the development of a framework to understand the root of the discrepancies in the measurement of the toughness of MGs and provide insights into the design of tough MGs for structural applications.

Keywords

Fracture energy, Metallic glass, Molecular dynamics simulation.

1. Introduction

Fracture toughness, also known as fracture energy or tearing energy, is an important material property and can be defined as the energy released with the extension of a crack per unit area. In most structural applications, the selection criterion for a material is commonly based on its toughness rather than its strength (Launey and Ritchie, 2009). Since the discovery of metallic glasses (MGs) in 1960 (Klement et al., 1960), they have been perceived as a quintessential class of structural materials (Ashby and Greer, 2006; Jang et al., 2013; Johnson, 1999). However, in contrast with crystalline materials, the toughness of MGs is relatively poorly understood. The challenge remains to accurately measure the toughness of MGs (Xu et al., 2010). Reported toughness values of MGs vary dramatically, from 2 $\mathrm{MPa}\sqrt{m}$ for Mg-based MGs to 200 $\mathrm{MPa}\sqrt{m}$ for Pd-based MGs (Demetriou et al., 2011; Lewandowski et al., 2005; Sun and Wang, 2015; Wang et al., 2007; Xi et al., 2005). In addition to this massive variation in toughness values among different MGs, large scatter in toughness values has also been found even for MGs within the same composition. For example, toughness values ranging from ~16 to ~130 $\mathrm{MPa}\sqrt{m}$ have been reported for $Zr_{41.2}Ti_{12.5}Cu_{10}Ni_{10}Be_{22.5}$ MG (Chen et al., 2015; Chen et al., 2017; Gilbert et al., 1999). The origin of the observed large variation in toughness is not well understood. Arguably, it may be caused by intrinsic effects, i.e., sample processing conditions, cooling rates, casting defects, and composition fluctuations (Chen et al., 2017; Garrett et al., 2012; Keryvin et al., 2006; Wang et al., 2012; Zhu et al., 2014). It may also be related to extrinsic effects such as test sample geometries and conditions, e.g. sample thickness and width, precision of notches, strain rates, and temperature (Chen et al., 2016; Chen et al., 2018; Lowhaphandu and Lewandowski, 1998; Wu et al., 2008). Therefore, establishing the relationships between these intrinsic and extrinsic factors and toughness will have direct implications for the commercial application of MGs as structural materials.

Accurate experimental measurements of MG toughness have been proven challenging. First of all, specific standards for measuring toughness of MGs are required such as ASTM E399 standard (ASTM E399-12, 2012). However, the sample dimension requirements are difficult to fulfill for the vast majority of MGs because fabrication methods such as casting and melt spinning have inherent limitations to the sample dimensions (Madge, 2015; Sun and Wang, 2015; Xu et al., 2010). In addition, it has been found that sample geometry characteristics such as thickness, width and notch radius have strong influences on the measured toughness of MGs (Chen et al., 2018). For instance, apparently toughness decreases with diminishing notch radius until a critical threshold value (Chen et al., 2016). In addition, it has been observed that sample processing conditions can significantly affect the toughness of MGs (Raut et al., 2018; Yuan et al., 2020). For instance, a lower cooling rate can lead to a decreased toughness value (Zhu et al., 2014). Thus, in general it is challenging to accurately measure the toughness of MGs in experiments because of the combined effects of intrinsic and extrinsic factors, i.e., sample processing conditions, sample geometries, and testing conditions (Chen et al., 2015; Xu et al., 2010). This is arguably the root of the widely divergent reported experimental measurements of toughness of MGs.

Within its limitations an atomistic modeling method such as molecular dynamics (MD) simulation allows for the decouple of the combined intrinsic and extrinsic effects, i.e., geometry and processing, on MGs' toughness measurements. In addition, MD enables independent and accurate control of individual parameters, thereby supporting a systematic and qualitative study. Atomistic simulations assessing the toughness of brittle materials have been reported previously (Gumbsch, 1995; Selinger and Farkas, 2000). Nonetheless, the insights and conclusions provided for brittle materials are not directly applicable to soft ductile materials. In addition, unlike crystalline metals, the characteristic material length scale over which crack instability occurs remains elusive in MGs due to their disordered atomic structure.

In terms of fracture behavior, MGs can be classified either as brittle or ductile. The fracture in brittle MGs, e.g., PdSi MGs, is governed by cracking mechanism (Moitzi et al., 2020), while the fracture in ductile MGs, e.g., CuZr MGs, is governed by shear banding (Wu et al., 2015). In MD simulations, however, it is not easy to classify MGs as ductile or brittle since most of the interatomic potentials are unable to describe accurately crack propagation. Nonetheless, recently, Moitzi et al. was able to simulate cracking in PdSi MGs with hybrid interatomic potentials including the many-body potential Embedded Atom Method (EAM) and Bond-Order potential calculations (Moitzi et al., 2020). Here, we focus on the fracture energy (G) measurement of the typical ductile $Cu_{50}Zr_{50}$ MGs. We measure the G of ductile MGs via MD simulations, by following the approach proposed by Deng *et al.* (Deng and Shi, 2018). The influences of sample processing, sample geometry, and testing conditions are systematically investigated. Correlations between these factors and the calculated value of G for CuZr MGs are established.

2. Simulation method

2.1. MD simulations

MD simulations are performed using the LAMMPS package (Plimpton, 1995; Zhao et al., 2009a; Zhao et al., 2009b). The EAM potential of Cheng et al. fitted to CuZr alloys is utilized to describe the interatomic interactions (Cheng et al., 2008). The CuZr samples are generated as follows. First, a small MG sample with dimensions of 6.2 × 6.2 × 6.2 nm^3 is prepared by melting a solid solution and thermalizing it at 2000 K. Then, the molten CuZr is quenched to 50 K at zero pressure using different quenching rates ranging from 3.4×10^{9} K/s to 3.4×10^{11} K/s (Lin et al., 2020; Sha et al., 2017a). The low temperature of 50 K is chosen in order to guarantee a regime of localized deformation despite the high strain rate and high cooling rate used (Sopu et al., 2017), as the glass structure model prepared from liquid quenching at a rapid cooling rate is more prone to thermal activations than real-world MGs that have experienced extended relaxation (Cheng et al., 2008). A large MG sample is then constructed by replicating the small representative MG system, which is then annealed at 800 K above the glass transition temperature (T_g) of 710 K (Sha et al., 2017b; Sha et al., 2017c) to minimize artificial patterns introduced during the replication process.

In order to measure the value of G for the different MG samples, we use the following procedure. CuZr MG samples with a narrow slab geometry and a single-edge notch are prepared as in the work of Deng and Shi (Deng and Shi, 2018), as shown in Fig. 1. The sample width (W) varies from 10 to 360 nm, while the length (L) is fixed at 31.2 nm and the thickness (B) is fixed at 6.2 nm. The notch depth is set at half of the sample width. After creating a 2.5-nm high edge notch, the notched MG samples are further relaxed for an additional 50 ps before loading. Once equilibration is attained, the top and bottom layers (~0.54 nm) in the *y*-direction, which are set as semi-rigid holders, are subjected to uniaxial tensile loading with strain rates ranging from 4.0×10^{7} s^{-1} to 1.0×10^{9} s^{-1}. In order to avoid unintended fracture near the rigid holders, atoms in the holder layers move rigidly in the *y*-direction yet are free to move in the *x*-*z* plane to avoid undesired stress concentration. During uniaxial tensile tests, periodic boundary conditions (PBCs) are applied along the *z*-direction, while free surfaces are present in the system in the *x* and *y*-directions.

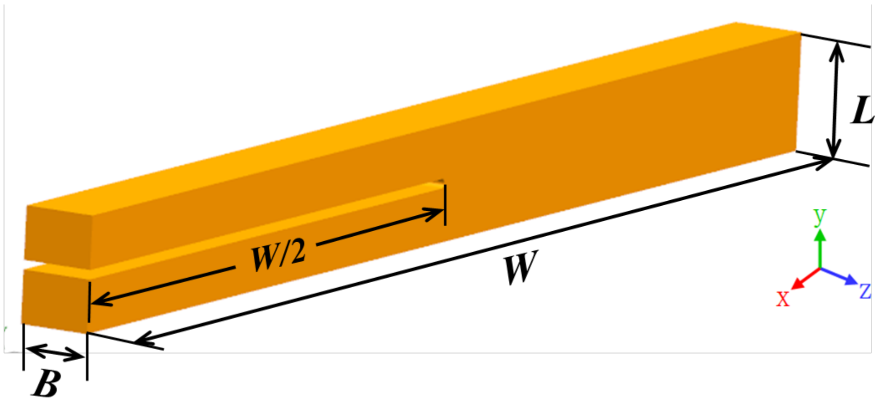

Figure 1. Illustration of the simulation model used to evaluate the fracture toughness of $Cu_{50}Zr_{50}$ MGs. The slab model features a pre-existing notch with depth set at half of the sample width.

2.2. Activation-relaxation technique

In this work, we employ the Activation-Relaxation Technique (ART) (Barkema and Mousseau, 1996; Malek and Mousseau, 2000; Mousseau et al., 2012) to investigate the activation barrier energy of MGs quenched at different rates. The ART is an efficient way to probe the potential energy landscape based on an open-ended saddle point search algorithm. The ART method proceeds in three steps: the initial minimum, its adjacent saddle point (activation), and the final minimum (relaxation) (Mousseau et al., 2012). The energy difference between the initial and final energy minimum states is calculated to be the activation energy. In our work, the sample sizes used in ART simulations are 3.3 × 3.3 × 3.3 nm^3, containing ~2000 atoms. The initial perturbation is introduced by imposing a random displacement of magnitude 0.5 Å to an atom. Next, the lowest eigenvalue of the Hessian matrix is evaluated by a Lanczos procedure. When the eigenvalue falls below -1.0 eV/ Å, the system will push towards a connecting saddle point along the direction of the lowest normalized eigenvector. Then, a saddle point state fulfilling the convergence criterion is obtained, when the total force in the system is less than 0.1 eV/ Å. The activation energy around each atom is calculated. For each MG sample, 10 ART searches with different random perturbation directions are employed.

3. Results and discussion

3.1. An approach to measure *G* in ductile MGs

Heretofore, there is a lack of a reliable method to directly measure G of MGs using MD simulations, particularly for ductile MGs. In MGs, cracks preferentially initiate at shear bands (SBs) in the plastic zone ahead of the notch root and then propagate along these bands until fracture. In this process, determining when the crack propagates is crucial for the measurement of G. However, the challenge is not only to simulate cracking in MGs but also to determine accurately when the crack propagates in an MD simulation, especially in the presence of a large amount of plastic deformation. To this end, we evaluate two approaches used by Chen *et al.* (Chen et al., 2018) and Deng *et al.* (Deng and Shi, 2018) in which they measured G for different MG models. Figure 2 illustrates the method employed to measure the value of G in Chen *et al.*'s work (Chen et al., 2018). Based on the load-displacement (*P*-*u*) curves for two specimens with the same sample thickness but slightly different notch depths (a_1 and a_2), the value of G is calculated as

$$G = \frac{\Delta \prod}{B(a_2 - a_1)} \tag{1}$$

where $\Delta \prod$ is the difference in the areas underneath the *P*-*u* curves, calculated at the critical displacement (u_c) at which crack extension occurs. In their MD simulations, $a_2 - a_1$ is taken as 1 nm, and the u_c is taken as the displacement at the maximum value of the applied force.

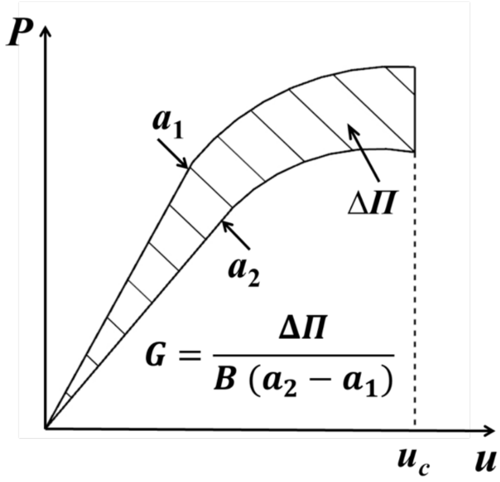

Figure 2. Illustration of the G measurement in Chen *et al.*'s work (Chen et al., 2018).

The method of estimating the value of G used in the MD simulations performed by Deng and Shi (Deng and Shi, 2018) is illustrated in Fig. 3. In this method two samples are used, one notched and one unnotched. The unnotched MG sample is used to measure the *P-u* curve, while the notched MG sample is used to determine u_c when crack extension occurs. The G can be determined as

$$G = \frac{\prod(u_c)}{BW} \tag{2}$$

where $\prod(u_c)$ is the work done to the unnotched sample up to u_c, calculated by the area beneath the *P-u* curve up to u_c. By monitoring the atomic number density (ρ_N) evolution ahead of the notch tip, u_c can be identified when ρ_N drops dramatically due to crack growth, as shown in Fig. 3(b). The determination of u_c implies that crack extension occurrence is very important for the measurement of G in MGs.

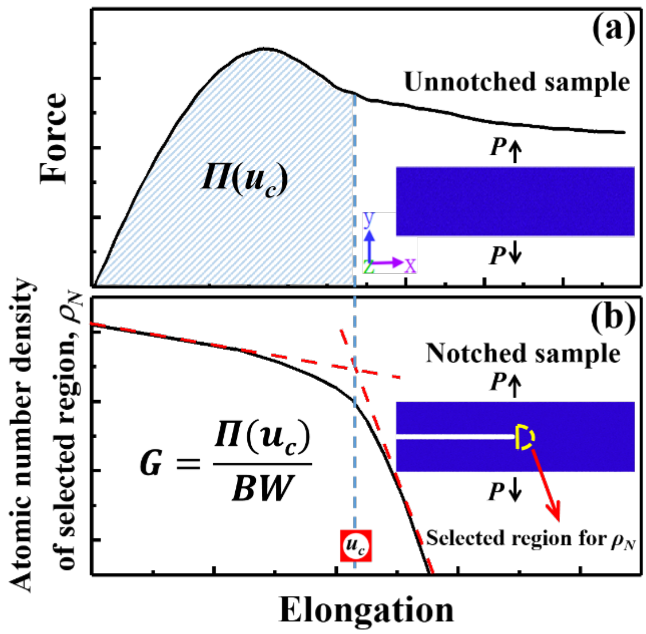

Figure 3. Illustration of the G measurement in Deng *et al.*'s work (Deng and Shi, 2018). (a) The unnotched sample is used to measure the *P*-*u* curve. (b) The notched sample is used to determine u_c. When the ρ_N ahead of the notch tip drops steeply, the crack extension occurs. u_c can be identified from the crossing point of the two linear fitting lines.

Taking a CuZr MG with the sample width of 360 nm as an example, the evolution of ρ_N ahead of the notch tip and the deformation patterns are shown in Fig. 4. ρ_N slowly decreases initially due to elastic dilation, and then drops sharply, indicating that the notch turns into a running crack. u_c can be identified from the crossing point of the two linear fitting lines. It should be noted that the crack process commonly observed in experiments is in contrast with that often observed in MD simulations due to the inherent different length scales. The crack process of bulk and miniature MG specimens involves transformation of one dominant SB into a crack (Flores et al., 2006). Tandaiya et al. have observed stable crack growth inside a dominant SB through a distance of ~60 μm (Tandaiya et al., 2013). They further showed that this length corresponds to the distance from the notch root over which a positive hydrostatic stress gradient prevails. Due to limited sample sizes as well as the lack of accurate interatomic potentials, it is challenging to simulate cracking in MGs through MD simulations (Moitzi et al., 2020).

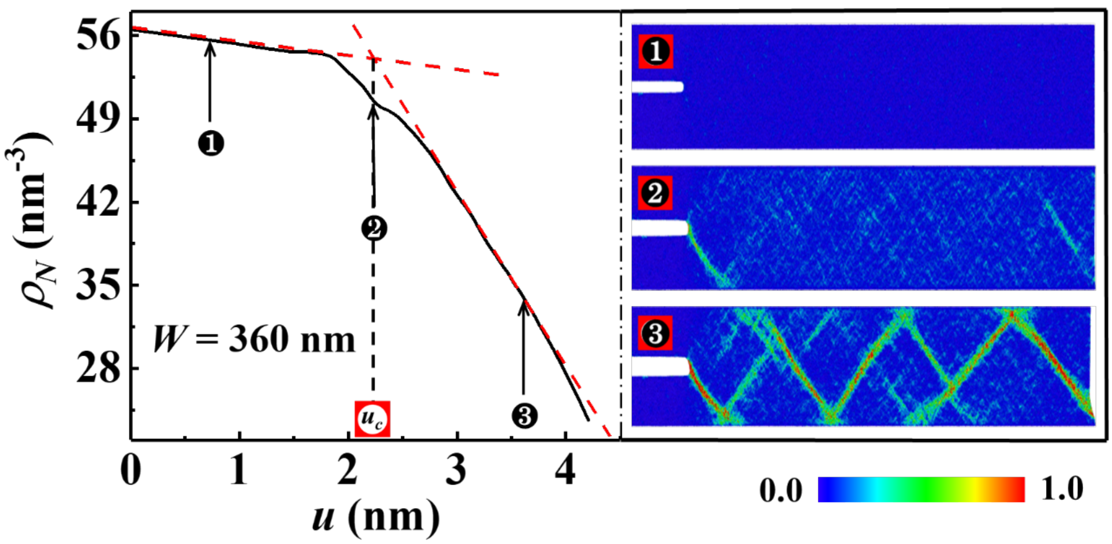

Figure 4. The ρ_N evolution during the crack extension for a CuZr MG with W = 360 nm. The insets are deformation patterns with each atom colored based on the atomic shear strain.

The effects of W on the measured G of ductile CuZr MGs evaluated by the above-mentioned two methods are shown in Fig. 5. In both methods, G shows a width-dependent behavior. The measured G values increase quickly when W increases from 10 to 50 nm. This G dependence on W can be understood from the perspective of the plastic zone size (R_P) at the notch root. When R_P is comparable to the un-cracked ligament length, G is sensitive to the un-cracked ligament length as it imposes a confinement effect on the plastic zone development and hence the strain energy release. In contrast, when R_P is negligible with respect to the un-cracked ligament, G is independent of *W*. Furthermore, it is shown that the measured G values by Deng *et al.*'s method are larger than those by Chen *et al.*'s method. In fact, for ductile MGs, a plastic zone is developed in the crack tip (Chen and Dai, 2016), and the released energy is dissipated in creating new crack surfaces as well as generating plastic deformation in the plastic zone. Thus, G should be written as (Sun and Wang, 2015; Zhu and Joyce, 2012)

$$G = G_p + 2\gamma \tag{3}$$

where G_p is the energy dissipated in plastic deformation and γ the surface energy. G_p is often much larger than 2γ, indicating that plasticity around the crack tip dominates the fracture behavior. As a result, the G values measured with the Deng and Shi's method are larger than those measured using the Chen *et al.*'s method, which only accounts for the surface energy contribution.

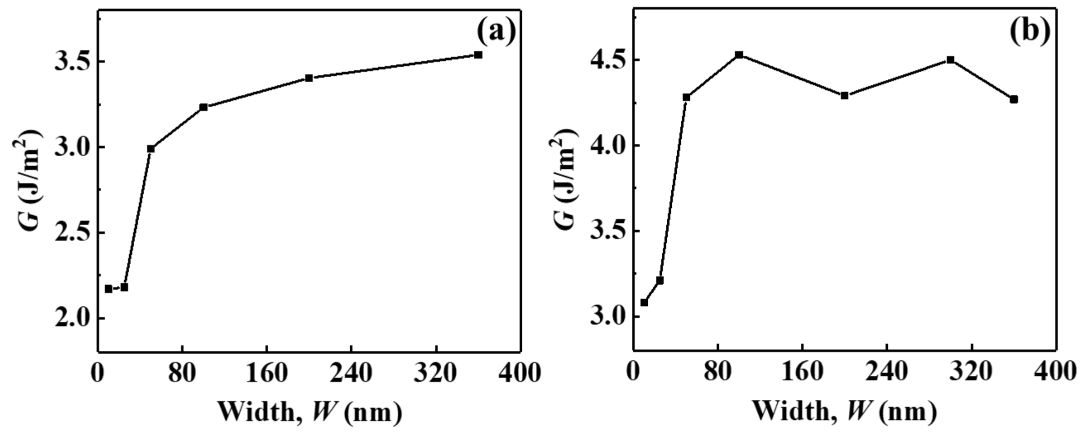

Figure 5. Sample width dependence of G of ductile CuZr MGs. (a-b) The measured

G values with sample widths ranging from 10 to 360 nm by Chen *et al.*'s method and Deng *et al.*'s method, respectively. The measured G values by Deng *et al.*'s method are larger than those by Chen *et al.*'s method in which they only consider the surface energy.

For plane strain, the relationship between G and the stress intensity factor (K) is defined as (Zhu and Joyce, 2012)

$$G = \frac{(1-\nu^2)K^2}{E} \tag{4}$$

where ν and E are the Poisson's ratio and the Young's modulus, respectively. Considering that R_p is expressed as (Deng and Shi, 2018)

$$R_p = \frac{1}{6\pi}\left(\frac{K}{\sigma_y}\right)^2 \tag{5}$$

where σ_y is the yield stress. Combining Eqs. (4) and (5), and considering the values $\nu = 0.35$, $E = 67.0$ GPa and $\sigma_y = 1.9$ GPa, estimated from our MD simulation of tensile loading on CuZr MGs (Sha et al., 2017c), we can calculate the value of R_p. For the large width sample ($W \geq 50$ nm) in Deng and Shi's and Chen *et al.*'s methods we obtain R_p~ 4.92 nm and R_p~3.4 nm, respectively. The R_p value obtained using Deng and Shi's method is close to the direct measurement of ~5.0 nm in our MD simulations. In view of the above discussion, Deng *et al.*'s approach is concluded to be the most suitable to estimate the value of G in ductile MGs. However, it is still to be determined what are the intrinsic and extrinsic effects such as the effect of cooling rate, strain rate, and temperature on the value of G. In the following sections, we systematically discuss the intrinsic and extrinsic effects on the calculated value of G for the ductile CuZr MG, by employing Deng *et al.*'s approach.

3.2. Effect of notch shape

Narayan et al. have systematically investigated the effects of specimen thickness, notch sharpness, and notch depth on the notch sensitivity of MGs (Narayan et al., 2018b). They found that the specimen thickness only mildly affects the strength of MGs, while the notch sharpness and notch depth have significant effects on the observed strength of MGs. Chen *et al.* have also demonstrated that notch radius is an important geometric parameter that can affect the toughness determination in MGs (Chen et al., 2016). It has been found that toughness decreases with diminishing notch radius until a critical value of dozens of μm. While below this critical value, toughness is independent of the notch radius. Here different notch shapes with fixed notch depths are used, including a rectangular notch, a semi-circular notch, and a semi-elliptical notch. The measured G values are 4.5, 4.27, and 4.41 J/m^2, respectively. However, it is noteworthy that the notch radii in our MD simulations are small. Due to the limitation of sample sizes in MD simulations, larger notch radii have not been considered. Arguably, the observed notch radius insensitivity originates from the small differences in notch radii among the different notch shapes considered. The semi-circular notch is hence employed in the following sections to study the effects of cooling rate, strain rate, and temperature.

3.3. Effect of cooling rate

The mechanical properties of MGs are strongly dependent on the structural states (Hu et al., 2001; Narayan et al., 2014). The cooling rate is a crucial parameter that influences the intrinsic amorphous structure of the MG sample, thus bearing direct relationship with the displayed toughness. To thoroughly examine the effect of cooling rate, we prepare CuZr MG samples at three different cooling rates in the range of 3.4×10^{9} K/s to 3.4×10^{11} K/s. The results show that the measured values of G increase with the cooling rate, as shown in Fig. 6(a). This tendency is consistent with recent experimental studies demonstrating that by increasing the cooling rate, the toughness of MGs is markedly elevated (Zhu et al., 2014). It is expected that the higher the cooling rate used in the preparation of a MG sample, the more free volume the sample will inherit from the liquid phase. Simulations and experiments have shown that a higher free volume level can lead to softer glasses, due to reduced shear and Young's modulus. On the other hand, it can also lead to higher plasticity, due to the reduced resistance to plastic deformation (Sun and Wang, 2015; Wang, 2012; Zhang et al., 2019). The measured *P-u* curves for CuZr MG samples obtained at three different cooling rates are shown in Fig. 6(b), suggesting that the maximal tensile force decreases for increasing cooling rate. Despite the reduced maximal tensile force, the calculated value of G increases, suggesting an increasing influence of the energy dissipated in the plastic deformation process. In MGs, shear transformation zones (STZs) are believed to be the carriers of plastic deformation. STZs can be monitored directly by using the atomic shear strain η_i^{Mises} (Shimizu et al., 2007). The presence of regions with relatively large atomic shear strain indicates a high density of STZs and the development of plastic deformation. The R_p can be quantitatively evaluated by measuring the fraction of atoms with relatively large atomic shear strain ($\eta_i^{Mises} > 0.2$) (Sha et al., 2013). The trend of the effect of cooling rate on the R_p is displayed in Fig. 6(c). R_p shows a similar cooling-rate dependence as G. As a result, the enhanced G is attributed to an increase in the value of R_p arguably caused by the large free volume level generated with the use of high cooling rates. The large free volume results in a decreased maximal tensile force, while it facilitates the generation and development of plastic deformation events.

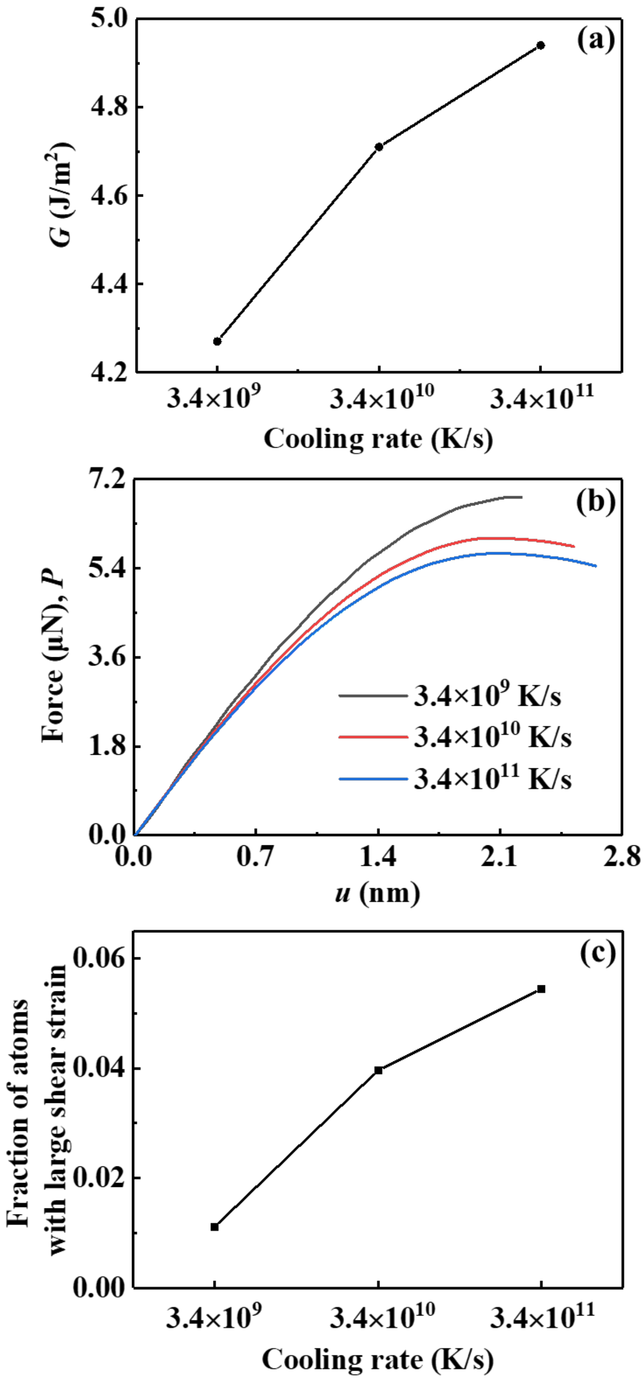

Figure 6. Dependence of the CuZr MG mechanical properties on the cooling rate. (a) Cooling-rate dependence of G. (b) P-u curves of samples obtained with three different cooling rates, indicating a decreased maximal tensile force for increasing cooling rates. (c) Fraction of atoms with relatively large atomic shear strain at the onset of crack extension, corresponding to the R_p, as a function of cooling rate.

Recently, Narayan et al. have successfully established a connection between the number of SBs and the fracture toughness of MGs (Narayan et al., 2018a). They have pinned down that the fracture toughness increases with the number of SBs by following a power law with an exponent of 1.5. Rajpoot et al. have come to similar conclusions investigating MG composites (Rajpoot et al., 2021). Due to the limitations of MD simulations length scale, the number of SBs ahead of the notch tip can't be captured and thus it is challenging to perform such analysis. However, motivated by previous findings and our current data, it is suggested that *G* should scale with the number of STZs, as shown in Fig. 6(a) and Fig. 6(c).

The STZs formation process, which mediates the plastic deformation is related to the local rearrangement of atomic clusters from the initial energy minimum position to an adjacent energy minimum position by overcoming an energy barrier. Atoms with low activation barriers are easy to rearrange during deformation, and STZ events are prone to activate. Here, we give a quantitative analysis of the activation energy barrier by the ART method. The dependence of activation energy on cooling rates is shown in Fig. 7(a-c). The results are consistent with previous reports (Fan et al., 2017; Şopu et al., 2020). The average activation energy of samples prepared with different cooling rates from 3.4×10^9 K/s to 3.4×10^{11} K/s are 1.5, 1.4, and 1.1 eV, respectively. The sample prepared at a high cooling rate experiences a low average activation energy barrier compared to the one prepared at a low cooling rate. Therefore, more STZs and plastic deformation are triggered in the fast quenched MG sample at comparatively similar stress loading. This result is consistent with the above analyses on the R_p.

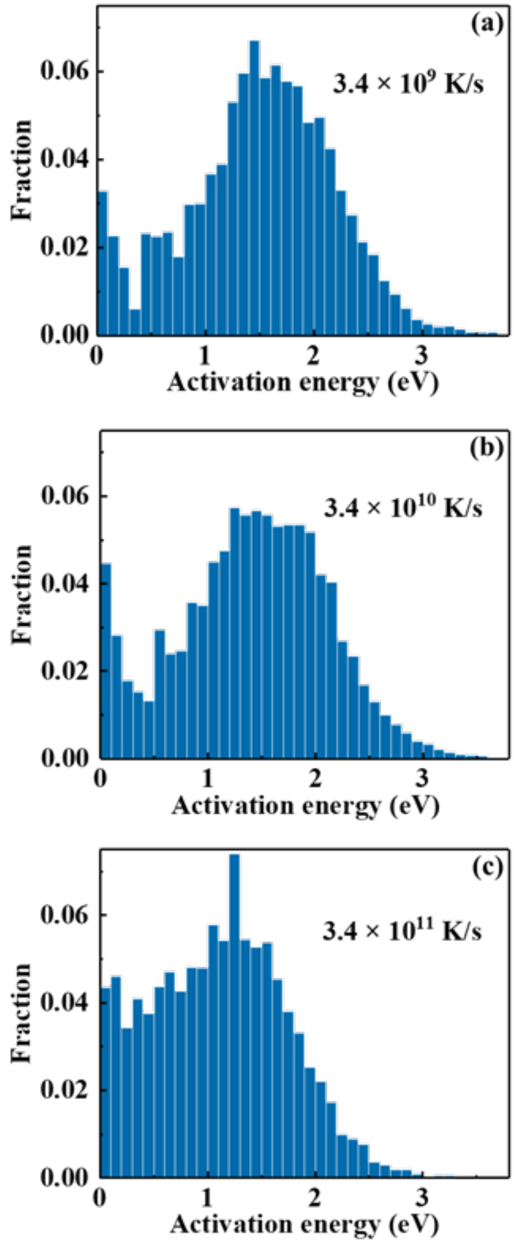

Figure 7. Histogram of the activation energy barrier for MGs quenched at different cooling rates as obtained by ART.

3.4. Effect of strain rate

It is worth noting that the mechanical properties of MGs are also dependent on the details of the loading tests (Sun and Wang, 2015; Yuan et al., 2020). Thus, it is important to discuss the extrinsic effect of the applied strain rate. The results show that the effect of strain rate on G is similar to that of the cooling rate, as shown in Fig. 8(a). The value of G noticeably increases with strain rate. However, the *P-u* curves, shown in Fig. 8(b), show that the maximal tensile forces are independent of the strain rates for rates below 1.0×10^{9} s^{-1}, suggesting that the physical origin of the strain rate-dependent G may stem from factors unrelated with the free volume. In contrast, it is found that u_c increases with strain rate, as depicted in Fig. 8(c). The u_c value has a significant effect on the measured value of G, as illustrated in Fig. 3. To accommodate the increase of plastic deformation at higher strain rates, many STZs activate simultaneously. However, the STZ aggregates accumulating at the notch root have to reach a critical SB nucleus size before the SB propagates triggering the onset of crack extension. Therefore, for higher strain rates, a larger strain, which corresponds to a greater u_c, is needed for SB nuclei to reach the critical length and propagate. As a result, the enhanced G can be attributed to the slow crack extension induced at high strain rates. Especially, at a strain rate of 1.0×10^{9} s^{-1}, both u_c and the tensile strength are increased, see Fig. 8(b). The results indicate that increasing strain rates restrict the time required for local relaxations and stress redistributions, raising the threshold stress for atoms to rearrange and form STZs.

In addition, the mechanical energy (estimated here by the summation of the kinetic and potential energies of the system) stored in the sample during the early stage of elastic deformation increases with the strain rate, as shown in Fig. 8(d). Greer and Sun suggested that the mechanical energy stored may induce damage and defects in MGs (Greer and Sun, 2016). Moreover, more stored energy indicates more energy available to activate STZs. Therefore, the increase of the mechanical energy can explain the observed enhanced G.

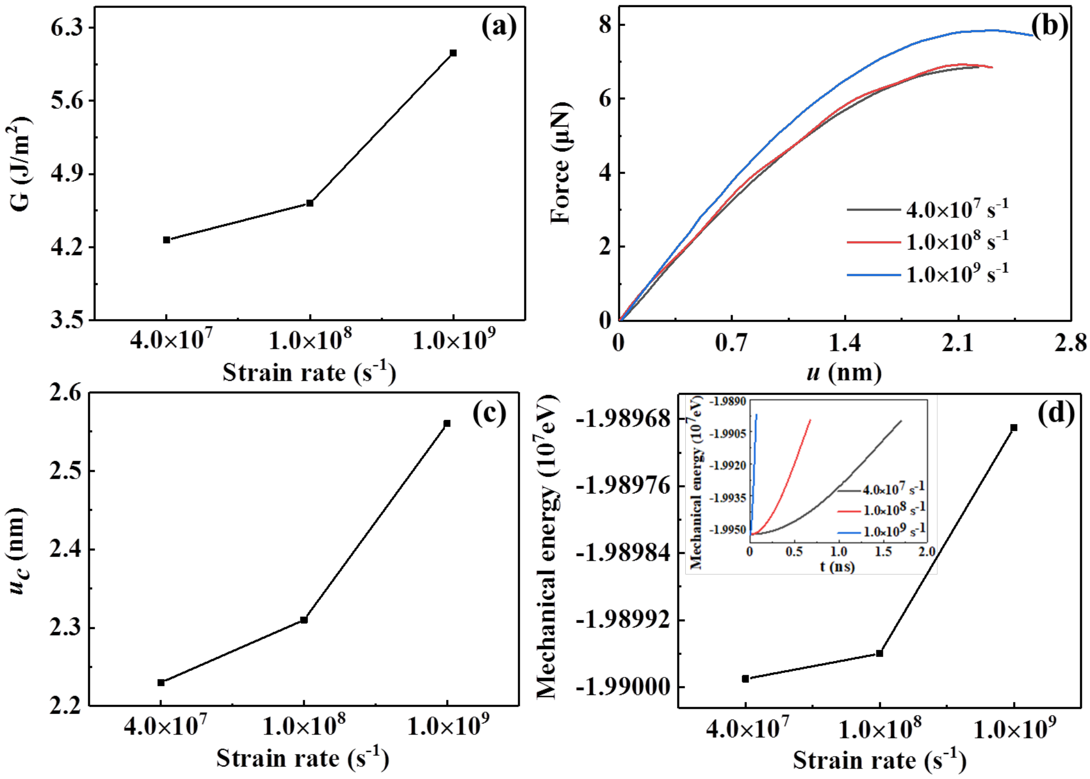

Figure 8. Dependence of the CuZr MG mechanical properties on the strain rate. (a) Strain-rate dependence of CuZr MG samples G. (b) *P-u* curves of CuZr MG samples subjected to different strain rates. (c) Measured u_c as a function of strain rate, showing correlation with the dependence displayed by G. (d) Mechanical energy stored in samples as a function of strain rate at the yield point. The inset shows the evolution of the mechanical energy of samples deformed at different strain rates before yielding.

3.5. Effect of temperature

Plastic deformation at its root involves an activation process over a transition energy barrier. Both thermal activation (i.e., temperature) and mechanical activation (i.e., stress) contribute to this process (Keryvin et al., 2008; Maaß and Löffler, 2015; Yuan et al., 2020). The temperature is a crucial parameter that influences the toughness of materials. Hence, in order to evaluate the effect of temperature in the toughness of CuZr MG we perform uniaxial tensile loading simulations considering different temperatures in the range from 50 to 600 K, which is below T_g of 710 K. It can be seen that the value of G dramatically decreases with increasing temperature, as shown in Fig. 9(a). On the one hand, the measured R_p as a function of temperature shown in Fig. 9(b) shows that the plastic deformation events increase with temperature. It is known that the plastic flow resistance of MGs decreases with increasing the temperature, since STZs activate abundantly with high thermal vibration (Yuan et al., 2020). The distributions of kinetic energy per atom in the sample at different temperatures are shown in Fig. 9(c), which are in agreement with recent MD simulation results (Yuan et al., 2020). The average kinetic energy of the system is shown to increase with temperature. All the kinetic energies are lower than 0.05 eV at 50 K, while more than 30% and 50% exceed 0.05 eV at 300 K and 600 K, respectively. That favors the STZs generation for increasing temperature, which is consistent with the above observation of the increased plastic deformation events with temperature shown in Fig. 9(b). Furthermore, it is noteworthy that the energy scale increases almost seven times from only 0.03 eV to about 0.2 eV by increasing temperature form 50 K to 300 K, while with further increasing temperature to 600 K the energy scale goes to only 0.4 eV. That indicates a decrease in the effect of phonon pumping at high temperatures.

On the other hand, the Young's modulus and strength decrease significantly with increasing temperature, as shown in Fig. 9(d). It is shown that as the temperature increases, the plasticity is improved to a certain extent, yet the strength is significantly reduced. This is because as the temperature increases, the STZ activation occurs at lower stress levels decreasing the strength accordingly. Since the value of G is determined by calculating the work done by the external load before crack propagation, it depends not only on the plastic deformation, but also on the tensile strength. As a result, the decreased G is attributed to a significant decrease in tensile strength at higher temperatures. In addition, the fracture of MGs can be regarded as the relative sliding of two solid planes on a thin layer of viscous fluid (i.e., a SB) (Gan et al., 2019; Maaß and Löffler, 2015). Higher temperatures reduce the viscosity of the shear zone, leading to softer MGs. The decrease in the viscosity of the shear zone may facilitate the relative sliding, reducing the energy required for crack advance, resulting in diminishing values of G as temperature increases.

Raut et al. have critically examined the temperature-dependence of fracture toughness of MGs (Raut et al., 2018). They have observed that the fracture toughness continuously decreases with increasing temperature from $0.4T_g$ to $0.67T_g$, which is followed by a continuous increase in the fracture toughness for further temperature increase. They attributed such non-monotonic variation of fracture toughness with temperature to the intermediate temperature ductility minimum (ITDM), which is a result of the transition in failure mechanism from SBs mediated plasticity to homogeneous deformation at high temperatures. Similarly, Wang et al. have also reported an ITDM in MGs (Wang et al., 2017). Interestingly, our MD simulation results contrast with these experimental findings by not showing an ITDM. However, it should be noted that the fracture behavior of MGs is size-dependent (Sorensen et al., 2020). The temperature threshold triggering the transition in failure mechanism in nanoscale MGs is arguably higher than that in bulk MGs, as the change in failure mechanism is not observed up to the temperature of 600 K considered in the MD simulations reported here.

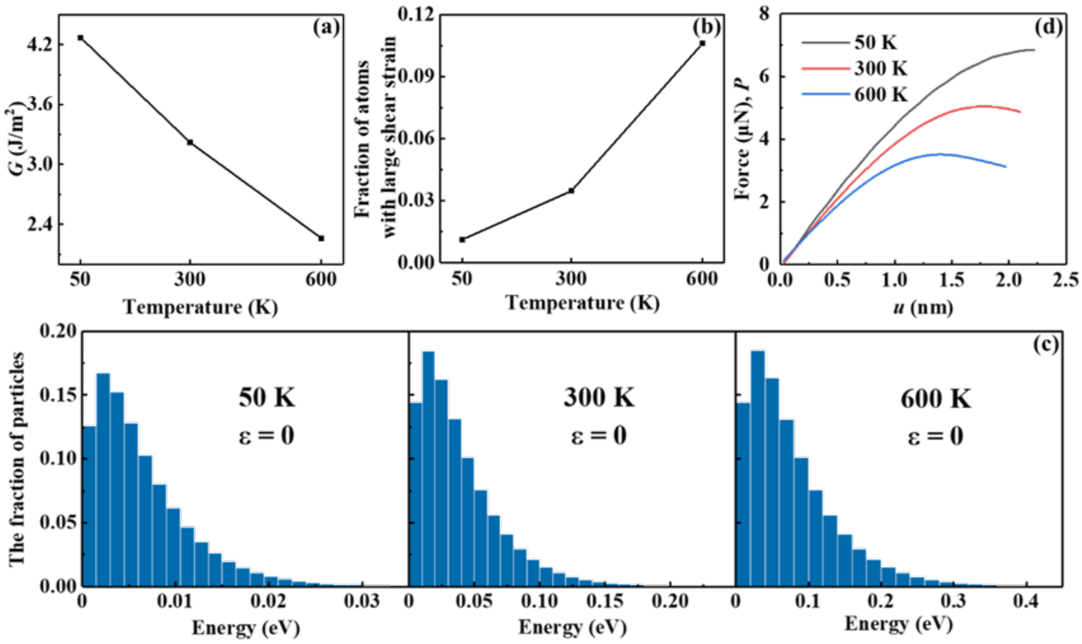

Figure 9. Temperature dependence of the CuZr MG properties with temperature. (a) Temperature dependence of CuZr MG G. (b) R_p as a function of temperature. (c) The distributions of kinetic energy per atom in the sample at different temperatures. (d) The P-u curves of CuZr MG samples subjected to different temperatures.

In the above, we have investigated the effects of sample geometries, sample preparation conditions, and loading conditions on the measurement of the fracture toughness of ductile MGs, as summarized in Table I. In view of our results, large G values are achievable when the MG samples are fabricated at high cooling rates and subjected to high strain rates. For example, the G value of CuZr MGs prepared at a cooling rate of 3.4×10^{11} K/s and subjected to a strain rate of 1.0×10^{9} s^{-1} is 6.48 J/m^2, which is ~ 1.5 times that of MGs prepared at a cooling rate of 3.4×10^{9} K/s and subjected to a strain rate of 4.0×10^{7} s^{-1}.

Table 1: Summary of calculated G values of CuZr MGs as a function of temperature, strain rate, cooling rate, notch shape, and notch dimensions.

MG	Temperature (K)	Strain rate (s^{-1})	Cooling rate (K/s)	Notch shape	Specimen width (nm)	Fracture toughness G (J/m^2)
$Cu_{50}Zr_{50}$	50	4.0×10^{7}	3.4×10^{9}	Semi-circle	10	3.08
					25	3.21
					50	4.28
					100	4.53
					200	4.29
					300	4.50
					360	4.27
	50	4.0×10^{7}	3.4×10^{9}	Rectangle	360	4.5
				Semi-circle		4.27
				Semi-ellipse		4.41
	50	4.0×10^{7}	3.4×10^{9}	Semi-circle	360	4.27
			3.4×10^{10}			4.71
			3.4×10^{11}			4.94
	50	4.0×10^{7}	3.4×10^{9}	Semi-circle	360	4.27
		1.0×10^{8}				4.62
		1.0×10^{9}				6.06
	50	4.0×10^{7}	3.4×10^{9}	Semi-circle	360	4.27
	300					3.22
	600					2.26
	50	1.0×10^{9}	3.4×10^{11}	Semi-circle	360	6.48

Before concluding, it is instructive to discuss the generality of our MD results. First of all, the strain rates and cooling rates employed in experiments differ from those used in MD simulations by many orders of magnitude. The small sample size used in MD simulations may also affect the deformation mechanisms. Thus we would like to point out that our MD results presented here have importance for advancing the understanding of toughness measurements of nanoscale MGs. In addition, the simulation results should be viewed with some skepticism because MD simulations are based on the type of empirical potentials. For these reasons, we focus on major mechanistic features and trends in behavior when interpreting MD simulation results.

5. Conclusions

One of the most important selection criteria for structural application materials is toughness. In this study, MD simulations are performed to measure the fracture toughness, G, of $Cu_{50}Zr_{50}$ MGs, with focus on the effects of cooling rate, notch shape, strain rate, and temperature. Correlations between the free volume, crack extension velocity and G have been established and highlight the effects of these intrinsic and extrinsic factors. Our results indicate that the highest values of G are achieved through a combination of processing at high cooling rates and deformation at high strain rates. This is attributed to the increased free volume in MGs produced at high cooling rates and the slow front propagation speed of SBs at high strain rates, both leading to increased energy dissipation through plastic deformation. Results additionally show a reduction in the value of G with increased temperature, arguably associated with a significant decrease in strength. The present study sheds light on the elusive origins of the influence of sample processing and loading conditions on the observed toughness of MGs and provides useful guidelines for the design of MGs with enhanced toughness for engineering applications.

Acknowledgments

H.L. and Z.D.S. would like to acknowledge financial support by the National Natural Science Foundation of China through Grant Nos. 11790293, 11972278 and 11772250. Z.D.S. is also grateful for the support from Science and Technology Developing Project of Shaanxi (2019JC-03). P.S.B. acknowledges support from the U.S. Department of Energy, Office of Science, Office of Basic Energy Sciences, under Award Number DE-SC0020295.

or favoring by the United States Government or any agency thereof. The views and opinions of authors expressed herein do not necessarily state or reflect those of the United States Government or any agency.

References

Ashby, M.F., Greer, A.L., 2006. Metallic glasses as structural materials. Scripta Mater. 54, 321-326.

ASTM E399-12, 2012. Standard Test Method for Linear-elastic Plane-strain Fracture Toughness KIc of Metallic Materials. ASTM International, West Conshohocken, PA, USA, pp. 1-33.

Barkema, G.T., Mousseau, N., 1996. Event-based relaxation of continuous disordered systems. Phys. Rev. Lett. 77, 4358-4361.

Chen, W., Ketkaew, J., Liu, Z., Mota, R.M.O., O'Brien, K., Da Silva, C.S., Schroers, J., 2015. Does the fracture toughness of bulk metallic glasses scatter? Scripta Mater. 107, 1-4.

Chen, W., Liu, Z., Ketkaew, J., Mota, R.M.O., Kim, S.-H., Power, M., Samela, W., Schroers, J., 2016. Flaw tolerance of metallic glasses. Acta Mater. 107, 220-228.

Chen, W., Zhou, H., Liu, Z., Ketkaew, J., Li, N., Yurko, J., Hutchinson, N., Gao, H., Schroers, J., 2017. Processing effects on fracture toughness of metallic glasses. Scripta Mater. 130, 152-156.

Chen, W., Zhou, H., Liu, Z., Ketkaew, J., Shao, L., Li, N., Gong, P., Samela, W., Gao, H., Schroers, J., 2018. Test sample geometry for fracture toughness measurements of bulk metallic glasses. Acta Mater. 145, 477-487.

Chen, Y., Dai, L.H., 2016. Nature of crack-tip plastic zone in metallic glasses. Int. J. Plast. 77, 54-74.

Cheng, Y.Q., Cao, A.J., Sheng, H.W., Ma, E., 2008. Local order influences initiation of plastic flow in metallic glass: Effects of alloy composition and sample cooling history. Acta Mater. 56, 5263-5275.

Demetriou, M.D., Launey, M.E., Garrett, G., Schramm, J.P., Hofmann, D.C., Johnson, W.L., Ritchie, R.O., 2011. A damage-tolerant glass. Nat. Mater. 10, 123-128.

Deng, B.h., Shi, Y.f., 2018. On measuring the fracture energy of model metallic glasses. J. Appl. Phys. 124, 035101.

Fan, Y., Iwashita, T., Egami, T., 2017. Energy landscape-driven non-equilibrium evolution of inherent structure in disordered material. Nat. Commun. 8, 15417.

Flores, K.M., Dauskardt, R.H., 2006. Mode II fracture behavior of a Zr-based bulk metallic glass. J. Mech. Phys. Solids 54, 2418-2435.

Gan, K.F., Jiang, S.S., Huang, Y.J., Yin, H.B.C., Sun, J.F., Ngan, A.H.W., 2019. Elucidating how correlated operation of shear transformation zones leads to shear localization and fracture in metallic glasses: tensile tests on Cu-Zr based metallic-glass microwires, molecular dynamics simulations, and modelling. Int. J. Plast. 119, 1-20.

Garrett, G.R., Demetriou, M.D., Chen, J., Johnson, W.L., 2012. Effect of microalloying on the toughness of metallic glasses. Appl. Phys. Lett. 101, 241913.

Gilbert, C.J., Schroeder, V., Ritchie, R.O., 1999. Mechanisms for fracture and fatigue-crack propagation in a bulk metallic glass. Metall. Mater. Trans. A 30, 1739-1753.

Greer, A.L., Sun, Y.H., 2016. Stored energy in metallic glasses due to strains within the elastic limit. Philos. Mag. 96, 1643-1663.

Gumbsch, P., 1995. An atomistic study of brittle fracture: toward explicit failure criteria from atomistic modeling. J. Mater. Res. 10, 2897-2907.

Hu, X., Ng, S.C., Feng, Y.P., Li, Y., 2001. Cooling-rate dependence of the density of $Pd_{40}Ni_{10}Cu_{30}P_{20}$ bulk metallic glass. Phys. Rev. B 64, 172201.

Jang, D., Maaß, R., Wang, G., Liaw, P.K., Greer, J.R., 2013. Fatigue deformation of microsized metallic glasses. Scripta Mater. 68, 773-776.

Johnson, W.L., 1999. Bulk glass-forming metallic alloys: science and technology. MRS Bull. 24, 42-56.

Keryvin, V., Bernard, C., Sanglebœuf, J.C., Yokoyama, Y., Rouxel, T., 2006. Toughness of $Zr_{55}Cu_{30}Al_{10}Ni_{5}$ bulk metallic glass for two oxygen levels. J. Non-Cryst. Solids 352, 2863-2868.

Keryvin, V., Prasad, K.E., Gueguen, Y., Sanglebœuf, J.C., Ramamurty, U., 2008. Temperature dependence of mechanical properties and pressure sensitivity in metallic glasses below glass transition. Philos. Mag. 88, 1773-1790.

Klement, W.K., Willens, R.H., Duwez, P., 1960. Non-crystalline structure in solidified gold-silicon alloys. Nature 187, 869-870.

Launey, M.E., Ritchie, R.O., 2009. On the fracture toughness of advanced materials. Adv. Mater. 21, 2103-2110.

Lewandowski, J.J., Wang, W.H., Greer, A.L., 2005. Intrinsic plasticity or brittleness of metallic glasses. Philos. Mag. Lett. 85, 77-87.

Lin, W.H., Teng, Y., Sha, Z.D., Yuan, S.Y., Branicio, P.S., 2020. Mechanical properties of nanoporous metallic glasses: insights from large-scale atomic simulations. Int. J. Plast. 127, 102657.

Lowhaphandu, P., Lewandowski, J.J., 1998. Fracture toughness and notched toughness of bulk amorphous alloy: Zr-Ti-Ni-Cu-Be. Scripta Mater. 38, 1811-1817.

Maaß, R., Löffler, J.F., 2015. Shear-band dynamics in metallic glasses. Adv. Funct. Mater. 25, 2353-2368.

Madge, S.V., 2015. Toughness of bulk metallic glasses. Metals 5, 1279-1305.

Malek, R., Mousseau, N., 2000. Dynamics of Lennard-Jones clusters: A characterization of the activation-relaxation technique. phys. Rev. E 62, 7723-7728.

Moitzi, F., Şopu, D., Holec, D., Perera, D., Mousseau, N., Eckert, J., 2020. Chemical bonding effects on the brittle-to-ductile transition in metallic glasses. Acta Mater. 188, 273-281.

Mousseau, N., Béland, L.K., Brommer, P., Joly, J.-F., El-Mellouhi, F., Machado-Charry, E., Marinica, M.-C., Pochet, P., 2012. The Activation-Relaxation Technique: ART Nouveau and Kinetic ART. J. At. Mol. Phys., 1-14.

Narayan, R.L., Raut, D., Ramamurty, U., 2018a. A quantitative connection between shear band mediated plasticity and fracture initiation toughness of metallic glasses.

Acta Mater. 150, 69-77.

Narayan, R.L., Tandaiya, P., Narasimhan, R., Ramamurty, U., 2014. Wallner lines, crack velocity and mechanisms of crack nucleation and growth in a brittle bulk metallic glass. Acta Mater. 80, 407-420.

Narayan, R.L., Tian, L., Zhang, D., Dao, M., Shan, Z.W., Hsia, K.J., 2018b. Effects of notches on the deformation behavior of submicron sized metallic glasses: Insights from in situ experiments. Acta Mater. 154, 172-181.

Plimpton, S., 1995. Fast parallel algorithms for short-range molecular dynamics. J. Comput. Phys. 117, 1-19.

Rajpoot, D., Narayan, R.L., Zhang, L., Kumar, P., Zhang, H., Tandaiya, P., Ramamurty, U., 2021. Shear fracture in bulk metallic glass composites. Acta Mater. 213, 116963.

Raut, D., Narayan, R.L., Tandaiya, P., Ramamurty, U., 2018. Temperature-dependence of mode I fracture toughness of a bulk metallic glass. Acta Mater. 144, 325-336.

Selinger, R.L.B., Farkas, D., 2000. Atomistic theory and simulation of fracture. MRS Bull. 25, 11-12.

Sha, Z.D., Branicio, P.S., Lee, H.P., Tay, T.E., 2017a. Strong and ductile nanolaminate composites combining metallic glasses and nanoglasses. Int. J. Plast. 90, 231-241.

Sha, Z.D., Pei, Q.X., Sorkin, V., Branicio, P.S., Zhang, Y.W., Gao, H.J., 2013. On the notch sensitivity of CuZr metallic glasses. Appl. Phys. Lett. 103, 081903.

Sha, Z.D., She, C.M., Xu, G.K., Pei, Q.X., Liu, Z.S., Wang, T.J., Gao, H.J., 2017b. Metallic glass-based chiral nanolattice: light weight, auxeticity, and superior mechanical properties. Mater. Today 20, 569–576.

Sha, Z.D., Wong, W.H., Pei, Q.X., Branicio, P.S., Liu, Z.S., Wang, T.J., Guo, T.F., Gao, H.J., 2017c. Atomistic origin of size effects in fatigue behavior of metallic glasses. J. Mech. Phys. Solids 104, 84-95.

Shimizu, F., Ogata, S., Li, J., 2007. Theory of Shear Banding in Metallic Glasses and Molecular Dynamics Calculations. Mater. Trans. 48, 2923-2927.

Şopu, D., Moitzi, F., Mousseau, N., Eckert, J., 2020. An atomic-level perspective of shear band formation and interaction in monolithic metallic glasses. Appl. Mater. Today 21, 100828.

Sopu, D., Stukowski, A., Stoica, M., Scudino, S., 2017. Atomic-Level Processes of Shear Band Nucleation in Metallic Glasses. Phys. Rev. Lett. 119, 195503.

Sorensen, D., Hintsala, E., Stevick, J., Pischlar, J., Li, B., Kiener, D., Myers, J.C., Jin, H., Liu, J., Stauffer, D., Ramirez, A.J., Ritchie, R.O., 2020. Intrinsic toughness of the bulk-metallic glass Vitreloy 105 measured using micro-cantilever beams. Acta Mater. 183, 242-248.

Sun, B.A., Wang, W.H., 2015. The fracture of bulk metallic glasses. Prog. Mater. Sci. 74, 211-307.

Tandaiya, P., Narasimhan, R., Ramamurty, U., 2013. On the mechanism and the length scales involved in the ductile fracture of a bulk metallic glass. Acta Mater. 61, 1558-1570.

Wang, C., Cao, Q.P., Wang, X.D., Zhang, D.X., Ramamurty, U., Narayan, R.L., Jiang, J.Z., 2017. Intermediate Temperature Brittleness in Metallic Glasses. Adv. Mater.

29, 1605537.

Wang, G., Zhao, D.Q., Bai, H.Y., Pan, M.X., Xia, A.L., Han, B.S., Xi, X.K., Wu, Y., Wang, W.H., 2007. Nanoscale periodic morphologies on the fracture surface of brittle metallic glasses. Phys. Rev. Lett. 98, 235501.

Wang, S.G., Sun, M.Y., Song, Z.Q., Xu, J., 2012. Cast defects induced sample-size dependency on compressive strength and fracture toughness of Mg–Cu–Ag–Gd bulk metallic glass. Intermetallics 29, 123-132.

Wang, W.H., 2012. The elastic properties, elastic models and elastic perspectives of metallic glasses. Prog. Mater. Sci. 57, 487-656.

Wu, F.F., Zhang, Z.F., Shen, B.L., Mao, S.X.Y., Eckert, J., 2008. Size effect on shear fracture and fragmentation of a $Fe_{57.6}Co_{14.4}B_{19.2}Si_{4.8}Nb_4$ bulk metallic glass. Adv. Eng. Mater. 10, 727-730.

Wu, Y., Bei, H., Wang, Y.L., Lu, Z.P., George, E.P., Gao, Y.F., 2015. Deformation-induced spatiotemporal fluctuation, evolution and localization of strain fields in a bulk metallic glass. Int. J. Plast. 71, 136-145.

Xi, X.K., Zhao, D.Q., Pan, M.X., Wang, W.H., Wu, Y., Lewandowski, J.J., 2005. Fracture of brittle metallic glasses: brittleness or plasticity. Phys. Rev. Lett. 94, 125510.

Xu, J., Ramamurty, U., Ma, E., 2010. The fracture toughness of bulk metallic glasses. JOM 62, 10-18.

Yuan, X., Şopu, D., Moitzi, F., Song, K.K., Eckert, J., 2020. Intrinsic and extrinsic effects on the brittle-to-ductile transition in metallic glasses. J. Appl. Phys. 128, 125102.

Zhang, M., Chen, Y., Li, W., 2019. On the origin of softening in the plastic deformation of metallic glasses. Int. J. Plast. 116, 24-38.

Zhao, K.J., Chen, C.Q., Shen, Y.P., Lu, T.J., 2009a. Molecular dynamics study on the nano-void growth in face-centered cubic single crystal copper. Comput. Mater. Sci. 46, 749-754.

Zhao, K.J., Fan, L.L., Chen, C.Q., 2009b. Multiaxial behavior of nanoporous single crystal copper: a molecular dynamics study. Acta Mech. Solida Sin. 22, 650-656.

Zhu, X.K., Joyce, J.A., 2012. Review of fracture toughness (G, K, J, CTOD, CTOA) testing and standardization. Eng. Fract. Mech. 85, 1-46.

Zhu, Z.D., Ma, E., Xu, J., 2014. Elevating the fracture toughness of $Cu_{49}Hf_{42}Al_9$ bulk metallic glass: effects of cooling rate and frozen-in excess volume. Intermetallics 46, 164-172.